

The Motzkin Spaghetti

Zhao Zhang^{1*}, and Olai B. Mykland²

¹ Department of Physics, University of Oslo, P.O. Box 1048 Blindern, N-0316 Oslo, Norway

²Department of Physics, Norwegian University of Science and Technology, NO-7491, Trondheim, Norway

* zhao.zhang@fys.uio.no

Abstract

While highly entangled ground states of gapless local Hamiltonians have been known to exist in one dimension, their two-dimensional counterparts were only recently found, with rather sophisticated interactions involving at least four neighboring degrees of freedom. Here, we show that similar bipartite entanglement properties can be realized on a square lattice with anisotropic interactions in four different quadrants. The interaction to generate such entanglement is much simpler than the previous constructions by coupling orthogonal arrays of highly entangled chains. The new construction exhibits an entanglement phase transition with different scalings of entanglement entropy at the critical point and in the lowly entangled phase, and faster decay of the spectral gap in the highly entangled phase. The tensor network representation of the new ground state consists of tensors with lower rank, while preserving a global geometry similar to that of the original networks.

Copyright attribution to authors.

This work is a submission to SciPost Physics.

License information to appear upon publication.

Publication information to appear upon publication.

Received Date

Accepted Date

Published Date

Contents

1	Introduction	2
2	The twisted Motzkin chain	4
3	Scaling of EE and spectral gap	5
4	Antiferromagnetic order in the radial direction	9
5	TN representation of the GS	10
6	Conclusion	13
A	Typical height change in a segment of Motzkin path	14
References		15

1 Introduction

Entanglement entropy (EE) is a measure of how entangled a quantum state is, or how different it is from a classical state. In that sense, the ground state (GS) of a locally interacting quantum many-body system separated by a spectral gap from the first excited state is not so different from a classical state, at least compared to generic eigenstates in the Hilbert space [1], as the EE of a subsystem grows with the size of the boundary instead of the bulk. This is known as the area law of EE [2], and is expected to hold in any spatial dimension. It is intuitive because massive quasiparticles propagate at a finite speed, resulting in exponentially decaying correlations. So only degrees of freedom within a finite range are effectively entangled across a boundary and contribute to the bipartite EE. The idea has been made rigorous into a proof for 1D systems using Lieb-Robinson bounds [3]. However, in 2D progress towards establishing a theorem has only been made for a certain class of Hamiltonians known as frustration free [4], to which the model proposed in this letter belongs.

What the area law does not tell us is how entangled a GS can be when the spectral gap closes, as happens in quantum criticality. There, the EE typically scales with an extra factor logarithmic in the subsystem size beyond the area law. This has been demonstrated with conformal field theories for (1+1)D critical points [5, 6], and with the Widom conjecture for gapless free fermions with a Fermi sea in arbitrary dimensions [7]. It is perhaps not so surprising as the correlation length typically scales linearly with the system size at critical points. But what was a little striking was that when the spectral gap decays even faster with the system size, for example at an exponential rate as opposed to the polynomial decay for critical systems, the EE can actually have a volume scaling. This was first exhibited in an inhomogeneously interacting XX spin chain [8–10], where the spins can be approximated to form Bell pairs symmetrically across the center in the GS, leading to maximal EE. The model was hence referred to as the rainbow chain.

Similar examples of highly entangled GSs with more exact descriptions were made possible with frustration free Hamiltonians [11], that are also translationally invariant (broken only by the finite boundary). For those Hamiltonians, the GS is simultaneously the lowest energy eigenstate of each local interaction operator, such that a lot can be known analytically about the GS by diagonalizing a few-body Hamiltonian. By mapping spin-1 configurations to discrete random walks, the GS of the critical Hamiltonian in Ref. [11] can be given as a superposition of Motzkin paths, those that start and end at height zero, without ever passing below it in the middle. Using combinatorial results, Bravyi et al. showed that the GS of the Motzkin chain has the same scaling behavior for EE, correlation and spectral gap as typical critical systems. Movassagh and Shor enlarged the local Hilbert space of the Motzkin chain with a color degree of freedom, which has a power law scaling of EE that outgrows the spin sector [12]. These constructions were later generalized to spin- $\frac{1}{2}$ systems, with smaller local degrees of freedom, but three-body interaction involving next-nearest neighboring sites [13, 14], giving its name Fredkin chain. To actually realize volume scaling in the GS, these Hamiltonians have to be deformed in a frustration free way, such that the GS superposition favors higher paths which allow more Bell pairs across the bipartition boundary [15–17]. As the deformation parameter is tuned, the GS undergoes an entanglement phase transition from area law to volume scaling.

It is not so straightforward to generalize the physical picture of Bell pair from 1D to 2D, as entanglement in two different directions competes against each other due to the monogamy of entanglement. Naive generalizations to the rainbow chain have been made in Ref. [10] and [18], which either exhibits volume scaling entanglement in only

one of the two directions on a square lattice, or along in both directions of a lattice of Hausdorff dimension one embedded in 2D space. The trade-off between entanglement in orthogonal directions was also exemplified in colored generalizations of the toric code model [19, 20], where enhanced entanglement along the bipartition boundary results in anomalous topological EE of the GS.

Another obstacle is a well-defined notion of height in 2D, when height differences can be counted along different paths connecting two points in the lattice. The prescription to fix both difficulties is to couple two orthogonal arrays of 1D Motzkin or Fredkin chains with appropriate vertex or tiling rules, such that a Coulomb gauge emerges to define an unambiguous height function [21, 22]. Moreover, the coupling leaves the Hamiltonian frustration free, and do not interfere with the interactions along each entangled chain. So unlike the anisotropic coupled wire construction of topological superconductors [23] where the inter-wire coupling opens up a gap, the system remains gapless. The resulting GSs are superpositions of discrete random membranes with a hard wall constraint at zero height, weighted by the deformation parameter to the power of the volume under the surfaces. The same entanglement phase transition occurs, except that the reduced height fluctuation in higher dimensions results in a logarithmic violation to the area law at the critical point instead of power law as in the 1D models.

While the six- or 19-vertex and lozenge tiling realizations appear to be the natural generalization of the highly entangled Motzkin (resp. Fredkin) chain to 2D, the support of the local Hamiltonian operators grows from two (resp. three) in 1D to four (resp. six). So while the paradigm in principle works for higher dimensions, the interactions become increasingly less realistic. There has also been a proposal of sequentially generable 2D coupled GS that is highly entangled in only one direction with local Hamiltonian operators having even larger support of eight [24]. An alternative loop-soup construction was proposed in Ref. [19], where the GS is a superposition of random loop configurations on a 2D lattice, and on each loop lives a periodic Motzkin chain [25]. However, due to the randomness of the loop configurations, it is not clear how the EE for any bipartition would actually scale with the subsystem size. Moreover, a naive generalization of the Motzkin Hamiltonian to periodic boundary conditions leaves the GS with exponential degeneracy [26], making a combination with exotic EE scaling trivially exist.

Both of those complications turn out to be absent with another route towards a well-defined height variable in 2D, namely by specifying a fixed path of counting height increments. For a traversal of the 2D plane along a path twisted from its center, this amounts to introducing anisotropic interactions on a square lattice along different directions in different quadrants. The choice of the neighboring degrees of freedom is such that their bond traces out a Motzkin chain twisted from its center. Since the location of the entangling degrees of freedom is fixed, the EE scaling property is analytically tractable from the asymptotic EE scaling behavior of segments of the Motzkin chain with lengths forming an arithmetic series. Like the EE scaling of the coupled-chain models, the bipartite EE of the current construction in the highly entangled phase scales with the volume of the subsystem regardless of the direction of the bipartition cut. But unlike the previous models, here EE obeys the area law at the critical point, and does not grow with the subsystem size in the lowly entangled phase.

The EE scaling of a quantum state is closely related to its tensor network (TN) representation. A TN with hierarchical structure for the Motzkin GS with logarithm violation of the area law proposed in Ref. [27] has recently been shown to be equivalent to a generalized multiscale entanglement renormalization ansatz (MERA) [28]. The equivalence was established by decomposing a rank-5 tensor, the minimal unit cell of the TN, into a product of rank-3 tensors and recombining them with their neighbors. Here, we perform

a similar reshaping of the TN for the volume entangled Fredkin chain inspired by the recently discovered holographic TN for the double-scaled SYK model [29]. By considering the conservation of arrow flows, we further optimize the tensors to a smaller set of configurations different on even and odd coordinates in the 2D bulk of the holographic TN. The new TN is then used to describe the GS of the current 2D model, showing global similarity with the previously obtained TN for the GS of the six-vertex coupled Fredkin chains [30].

The rest of the article is organized as follows. Sec. 2 defines the model with highly entangled GS in two directions by filling a 2D square lattice with a Motzkin chain twisted from the center. Sec. 3 analyzes the asymptotic scaling of the EE by mapping bipartitions of the 2D system into disjoint segments along the 1D chain. The result together with the scaling behavior of spectral gap converted from the 1D results for different phases and the critical points are compared with those for the previous coupled-chain constructions. Sec. 4 highlights the induced antiferromagnetic order in the spin sector along the radial direction of the 2D lattice. Sec. 5 introduces a new TN representation of the highly entangled 1D chains, the 2D twisted version of which is compared with the genuine 2D TN with similar global structure. Finally, a conclusion is given in Sec. 6 with outlook on higher dimensional generalizations and EE scaling laws for gapless GSs.

2 The twisted Motzkin chain

The q -deformed bicolor Motzkin chain [15] has a five-dimensional local Hilbert space, with spin up and down, both in either red (r) or blue (b) color, and a colorless spin zero. The Hamiltonian is expressed in terms of projectors

$$P_j^c = |L^c\rangle_{j,j+1}\langle L^c|_{j,j+1} + |R^c\rangle_{j,j+1}\langle R^c|_{j,j+1} + |F^c\rangle_{j,j+1}\langle F^c|_{j,j+1}, \quad (1)$$

where

$$\begin{aligned} |L^c\rangle_{j,j+1} &= \frac{1}{\sqrt{1+q^2}} \left(|\uparrow_j^c 0_{j+1}\rangle - q |\downarrow_j^c 0_{j+1}\rangle \right), \\ |R^c\rangle_{j,j+1} &= \frac{1}{\sqrt{1+q^2}} \left(|0_j \downarrow_{j+1}^c\rangle - q |\downarrow_j^c 0_{j+1}\rangle \right), \\ |F^c\rangle_{j,j+1} &= \frac{1}{\sqrt{1+q^2}} \left(|\uparrow_j^c \downarrow_{j+1}^c\rangle - q |\downarrow_j^c 0_{j+1}\rangle \right). \end{aligned} \quad (2)$$

Each of the projection operators has a local lowest energy eigenstate corresponding to the direction orthogonal to the above three vectors. So the GS of a Hamiltonian consisting of such projectors acting on all neighboring pairs of sites in the chain is a weighted superposition of random walks if the up, down and 0 spins are respectively mapped to up, down and flat moves. In addition to the color matching encoded in $|F^c\rangle_{j,j+1}$ between up and down moves when they are pair created from spin zeros, an energy penalty needs to be introduced by the projector $C_j^{c_1,c_2} = |\uparrow_j^{c_1} \downarrow_{j+1}^{c_2}\rangle \langle \uparrow_j^{c_1} \downarrow_{j+1}^{c_2}|$ for $c_1 \neq c_2$ in order to enforce color matching between nearest up-down pairs in the GS configurations. The remaining GS degeneracy can be lifted by fixing the boundary conditions with the Hamiltonian $H_\partial = \sum_{c=r,b} |\downarrow^{c_1}\rangle \langle \downarrow^{c_1}|_1 + |\uparrow^{c_1}\rangle \langle \uparrow^{c_1}|_{2N}$. In summary, the Motzkin Hamiltonian is given by

$$H = H_\partial + \sum_{j=1}^{2N-1} \left(\sum_{c=r,b} P_j^c + \sum_{c_1 \neq c_2} C_j^{c_1,c_2} \right). \quad (3)$$

It has a unique GS as a superposition of spin configurations where there is always at least as many up spins as down spins to the left at any point along the chain, and the colors of the nearest up-down spins pairs are either both red or both blue, in a nested fashion. If up (resp. down) spins are mapped to 45° upward (resp. downward) moves with unit horizontal lengths, and the area enclosed between a Motzkin path m and the horizontal axis at height zero is denoted $A(m)$, then up to an overall normalization factor, the GS can be expressed as

$$|\text{GS}\rangle = \sum_{m \in M_{2N}} q^{A(m)} |m\rangle, \quad (4)$$

where M_{2N} denotes the set of bicolor Motzkin paths of length $2N$ with color matching.

Since the anisotropic 2D model is constructed by twisting a 1D chain with a length that is quadratic in the linear size of the 2D lattice, we only need to specify the bonds on the 2D lattice occupied by degrees of freedom along the 1D chain. This is shown in Fig. 1 (a), where the colored spins reside on the lattice sites of an 9×8 square lattice, with Motzkin interaction turned on along the solid edges tracing out a Motzkin chain beginning at the northwest corner and ending at the southeast corner of the lattice. Alternatively, the spins can live on the edges of the square lattice covered by the twisted Motzkin chain, and interactions are only turned on between adjacent spins on the chain, as shown in Fig. 1 (b). Depending on the location of the spin in the square lattice, it can be either between east-west (resp. north-south) neighbors for the upper and lower (resp. left and right) quadrants. Near the two diagonal lines, where the winding 1D chain turns, the interaction is between neighbors around a corner. The two layouts of the spins and neighboring interactions are asymptotically equivalent in terms of the scaling behavior of bipartite EE. However, the latter has a more regular distribution of segments along the Motzkin chain, so for convenience we will work with this lattice in the following.

To study the isotropic EE, four symmetric bipartition cuts are shown in Fig. (1) (a) and (b). They separate the spins into two subsystems consisting of increasingly larger segments of size $4n - a$, for $n = 1, 2, \dots, L/2 + 1$, with $a = 0, 1, 2, 3$ corresponding respectively to the yellow, blue, green and red cut. Starting from the center, segments within one subsystem in the 2D lattice on a given side of the cut alternate between the first and second halves of the 1D chain when it is stretched straight. Obviously the scaling behavior of bipartite EE for any of the cuts will not differ qualitatively, so from now on we focus on the yellow cut along the main diagonal with $a = 0$, which results in a bipartition shown in Fig. (1) (b).

3 Scaling of EE and spectral gap

As analyzed in Ref. [15], the EE of the Motzkin GS decomposes into a leading contribution from the color degree of freedom, and a subleading contribution from the spin sector. Only up-down spin pairs belonging to different subsystems account for the former. In the Motzkin path picture, this means that only the net height change of a subsystem, or the surplus of up spins matters. For the 1D system studied there, the leading contribution to the EE is therefore proportional to the height at the center of the Motzkin path, giving the three distinct scaling behaviors in the two different phases and the critical point. For the critical point at $q = 1$, the EE of a single connected segment in the middle of the chain has also been obtained from combinatorial analyses for the colorless [31] and colored Motzkin chains [32]. Here, the situation seems a bit more complicated, as segments belonging to two subsystems alternate along the chain. A rigorous estimation would rely on the enumeration of Motzkin-like paths that stay within the upper half plane but starts and

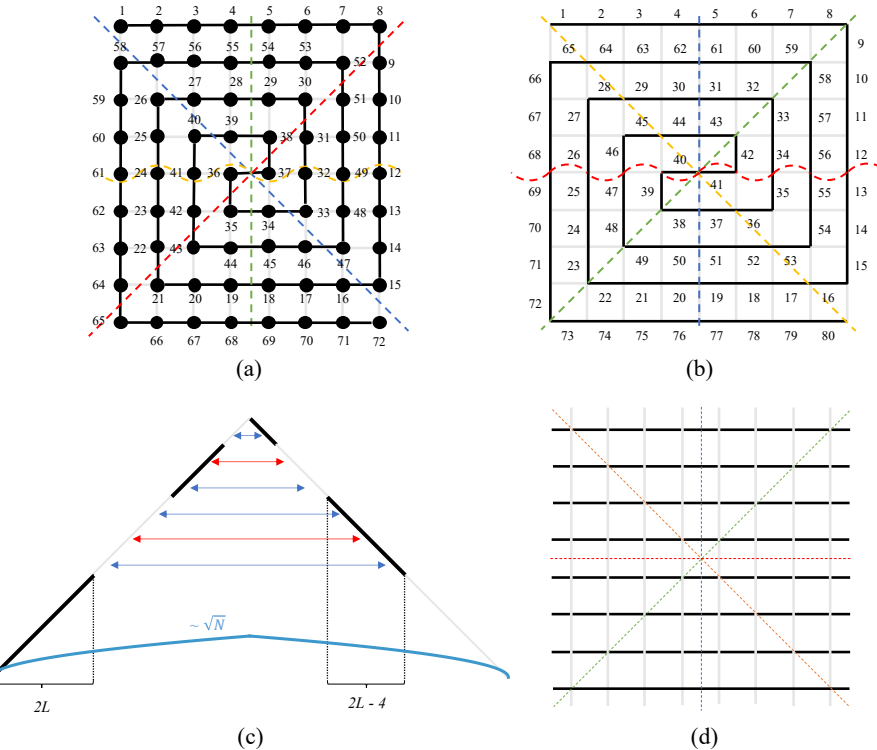


Figure 1: (a) A square lattice with $L(L+1)$ spins on the vertices. (b) An $L \times L$ square lattice with spins on the edges of the square lattice that are covered by a Motzkin chain of length $2N = L(L+2)$, both shown here for $L = 8$. Four symmetric bipartition cuts are shown in different colors. (c) The two subsystems resulting from the yellow cut in (b). The northeast subsystem is represented with the thickened black lines, whereas the southwest is marked by thin gray lines. This is asymptotically equivalent to the yellow bipartition in (a), separating the upper half plane from the lower. The configuration depicted corresponds to the probabilistically dominant Motzkin path in the GS superposition for the $q > 1$ phase, to illustrate the entanglement across subsystems. Typical height configuration at the critical point is depicted in blue. (d) The uncoupled arrays of orthogonal chains with different EE and gap scaling for comparison in Table 1 and Table 2.

ends at nonzero height. In Appendix A, we point out the challenge of a rigorous estimation from the combinatorial and path-integral perspective.

The decomposition of EE into a color contribution and a height fluctuation contribution can be seen from the Schmidt decomposition of the GS

$$|\text{GS}\rangle = \sum_{c, \delta h} \sqrt{p_{\delta h, c}} |A_{\delta h, c}\rangle \otimes |B_{\delta h, c}\rangle \quad (5)$$

where the Schmidt coefficient $p_{\delta h, c}$ depends on the total height changes $\delta h = [\delta h^1, \delta h^2, \dots]$, where each entry refer to the height change of a segment resulting from the cut across the 2D lattice, and the coloring c of the surplus up- or down-spins that are paired between the two subsystems A and B . Since the number of such pairs across subsystems depend on the height changes, the joint probability $p_{\delta h, c}$ is the marginal probability $p_{\delta h} = \sum_c p_{\delta h, c}$ times the conditional probability $p_{c|\delta h} = p_{\delta h, c}/p_{\delta h}$. The resulting entropy can therefore

be written as

$$\begin{aligned}
S(\{p_{\delta h, c}\}) &= - \sum_{c, \delta h} p_{\delta h, c} \log p_{\delta h, c} \\
&= - \sum_{c, \delta h} p_{\delta h} p_{c|\delta h} (\log p_{\delta h} + \log p_{c|\delta h}) \\
&= - \sum_{\delta h} p_{\delta h} \sum_c p_{c|\delta h} \log p_{c|\delta h} - \sum_{\delta h} p_{\delta h} \log p_{\delta h} \sum_c p_{c|\delta h} \\
&\equiv \sum_{\delta h} p_{\delta h} S_c(\delta h) - \sum_{\delta h} p_{\delta h} \log p_{\delta h} \\
&= \langle S_c \rangle + S_h.
\end{aligned} \tag{6}$$

Assuming that the spins in each segment are always paired with those in the other subsystem, instead of other segments in the same subsystem, with the opposite sign of total spin, the conditional probability is simply $p_{c|\delta h} = \prod_s 2^{-\delta h^s}$, where the superscript s labels the segments in subsystem A . This follows from the fact that the two colors are equally likely. This is indeed the paths with the largest $p_{\delta h}$ in the scaling limit, as the height function is monotonic in the two halves of the chain, as shown in Fig. (1) (c). Since we are interested in the scaling behavior of EE, even though there is a certain probability that some segments will end up pairing up in color inside the same subsystem, the color contribution averaged over the height distribution can still be estimated as

$$\langle S_c(\delta h) \rangle = - \sum_c \langle p_{c|\delta h} \log p_{c|\delta h} \rangle = \log 2 \sum_s |\delta h^s|. \tag{7}$$

This is in proportion to the the total height change in the subsystem.

Instead of evaluating the path integral Eq. (A.5) by brute force, we will use the known results on the asymptotic scaling of the height function. For $q = 1$, the height at distance x away from the endpoint $h_k = \sum_{i=1}^k S_i^z$ on average scales as $\langle h_k \rangle \sim \sqrt{k}$ in the continuous limit [15, 16], which is due to the repellent hard wall at height 0. For the particular bipartition in question, we can further use the symmetry about the midpoint $\langle h_k \rangle = \langle h_{L-k} \rangle$ to write Eq. (A.5) as

$$S \sim \sum_{k=1}^{\frac{L}{2}} (-1)^k \langle h_{k-1} \rangle + \sum_{k=\frac{L}{2}}^{L-1} (-1)^k \langle h_{L-k} \rangle = \langle h_{\frac{L}{2}} \rangle = \sqrt{\sum_{j=0}^{\frac{L}{2}-1} (2L - 4j)} = \sqrt{L^2 + 2L}, \tag{8}$$

which scales linearly with L asymptotically. In fact, this is nothing but the average height at the middle of the chain, meaning that the bipartite EE of the 2D lattice of linear size L scales in the same way as the EE of half chain with length L^2 .

For the $q > 1$ phase, $\langle h_k \rangle \sim k$, so a completely analogous argument gives the scaling $S \sim L^2$. The $q < 1$ phase, on the other hand, has a bounded height everywhere $\langle h_k \rangle \sim \mathcal{O}(1)$, which results in the scaling $S \sim \mathcal{O}(1)$. Notice that this EE is significantly sub-area law, reminiscent of the colorless version of the coupled chain models [21, 22], and more severe than the topological and logarithmic corrections of the colored loop models studied in Ref. [20].

To estimate the EE scaling in the various phases of the Motzkin GS we can also use its matrix product state (MPS) representation, found in Ref. [28]. By summing up the absolute value of the height differences Δ_s across segments s in one of the subsystems defined by one of the cuts in Fig. (1), we can estimate the EE S . That is

$$S \sim \sum_{s \in \mathcal{S}_{\text{cut}}} |\Delta_s| = \sum_{s \in \mathcal{S}_{\text{cut}}} |\langle h_f^s - h_i^s \rangle|, \tag{9}$$

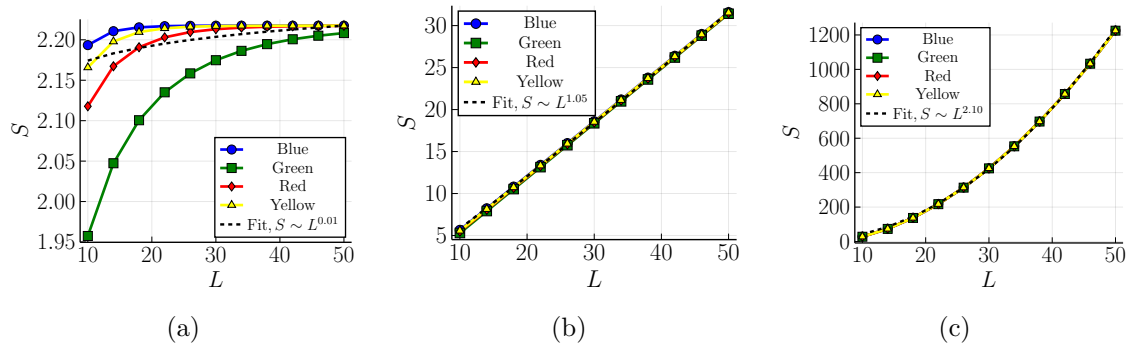


Figure 2: Scaling of the bipartite EE S computed from Eq. (9) and the MPS representation of the GS for various linear system sizes L and for the different colored cuts in Fig. (1) (a). In (a) $q = 0.99$, in (b) $q = 1$ and in (c) $q = 1.01$.

where \mathcal{S}_{cut} contains all segments in one of subsystems defined by one of the colored cuts in Fig. (1) (a) and h_i^s (resp. h_f^s) is the height at the beginning (resp. end) of the segment s . For example, if we consider the blue cut in Fig. (1) (a) and the northeast subsystem, \mathcal{S}_{cut} will consist of segments $[1 \dots 15]$, $[47 \dots 57]$, $[27 \dots 33]$ and $[37, 38, 39]$. In each of the segments, h_i^s and h_f^s is the height at the spin denoted by the first and the last number respectively. Note that Eq. (9) is identical with the first form of Eq. (A.5). The expected height values $\langle h \rangle$ are computed from the MPS representation. This gives the plots in Fig. (2). Clearly, the scaling in the various phases matches the above results and are independent on the exact bipartition considered in the large L limit.

The subleading contribution to the EE is from the fluctuation in the height of Motzkin paths, which is also the sole source of entanglement for a monochromatic version of the model. A Schmidt decomposition of the reduced density matrix shows that the two subsystems only depend on each other via the total spin within one subsystem, such that the total spin of the whole chain is zero. Moving from the 1D system to our 2D construction, nothing changes except the subsystem is distributed into disconnected segments. So the dimensionality of the reduced density matrix is still the number of possible values of the total spin. However, in the $q > 1$ (resp. $q < 1$) phase, the probability of the total spin, or height change decays exponentially with the deviation of the area underneath a Motzkin path from the most probable one that is of highest height (resp. completely flat) [15, 16]. So only paths with a height change at finite distance away from the typical one effectively matters, giving a contribution to the EE from height fluctuations that is a bounded constant independent of system size for both phases. When $q = 1$, there is more fluctuation. Although entropic repulsion pushes the average height to order \sqrt{N} above the hard wall at zero height, the variance of the Gaussian free field remains to scale linearly with the total length of the segments, making the EE scale as $\log N$ [11]. Note that in a monochromatic version of the 2D model, all three scalings are sub-area law, which is unique to our construction of filling the 2D lattice with a twisted 1D chain.

It is worth comparing the EE scalings of the two different 2D models together with a quasi-1D model composed of two layers of Motzkin chains in orthogonal directions that are not interacting with each other, as shown in Fig. (1) (d). Such a construction correspond to yet another way to define height function in 2D, namely by the Cartesian product of heights along the chains in two different directions. Since the chains in each layer are neither interacting with one another, nor with those in the other direction, the EE scaling in both phase and the at the critical point are simply the corresponding scaling of a single 1D chain multiplied by L , as summarized in Table. 1.

Table 1: Comparison of the EE scalings with linear system size L between the two different 2D constructions and the quasi-1D arrays of uncoupled chains.

Model	Phase	Coupled chains	Twisted chain	Uncoupled chains
Colored	$q > 1$	L^2 [21, 22]	L^2	L^2
	$q = 1$	$L \log L$ [21, 22]	L	$L^{\frac{3}{2}}$
	$q < 1$	L [21, 22]	$\mathcal{O}(1)$	L
Colorless	$q > 1$	$\mathcal{O}(1)$	$\mathcal{O}(1)$	L
	$q = 1$	L ¹	$\log L$	$L \log L$
	$q < 1$	$\mathcal{O}(1)$	$\mathcal{O}(1)$	L

Unlike the scaling of EE discussed above, which requires somewhat different analyses than the 1D system due to the more complicated bipartition, upper-bounds on the scaling of the spectral gap can be straightforwardly deduced from the 1D scaling simply by substituting the linear system size with $N = L(L + 2)$. The results are summarized in [Table. 2](#). This should be compared with the EE scaling in [Table. 1](#). In particular, the $q > 1$ phase of the colored model shows that the same EE scaling does not imply the same scaling of spectral gap, and vice versa as shown by the critical point of the colored model.

Table 2: Comparison of the spectral gap scalings with linear system size L between the two different 2D constructions and the quasi-1D arrays of uncoupled chains, where asterisks denote conjecture scalings. The greek letters denote different positive constants.

Model	Phase	Coupled chains	Twisted chain	Uncoupled chains
Colored	$q > 1$	$e^{-\alpha L^3}$ [21]	$e^{-\beta L^4}$ [17, 34]	$e^{-\beta L^2}$ [17, 34]
	$q = 1$	$L^{-\gamma*}$ [30]	$L^{-2\delta}$ [12]	$L^{-\delta}$ [12]
	$q < 1$	$\mathcal{O}(1)^*$ [30]	$\mathcal{O}(1)$ [35]	$\mathcal{O}(1)$ [35]
Colorless	$q > 1$	$e^{-\epsilon L^2}$ [21]	$e^{-\zeta L^2}$ [17, 34]	$e^{-\zeta L}$ [17, 34]
	$q = 1$	$L^{-\eta*}$ [30]	$L^{-2\theta}$ [11]	$L^{-\theta}$ [11]
	$q < 1$	$\mathcal{O}(1)^*$ [30]	$\mathcal{O}(1)$ [35]	$\mathcal{O}(1)$ [35]

4 Antiferromagnetic order in the radial direction

Although the twisted 1D chain fills the entire 2D lattice in our construction, one might argue that the system is not a genuine interacting in 2D, as there are no couplings between adjacent segments of the 1D chain within each quadrant of the lattice. The caveat in that argument is that the coupling within different quadrants are along different directions,

¹This is an upper-bound from the zeroth order Rényi entropy. The random membrane when bipartitioned gives a Motzkin path on the boundary, giving the dimensionality of the reduced density matrix. The same upper-bound was also obtained for six-vertex models with domain wall boundary conditions using the exact enumeration of alternating sign matrices [33].

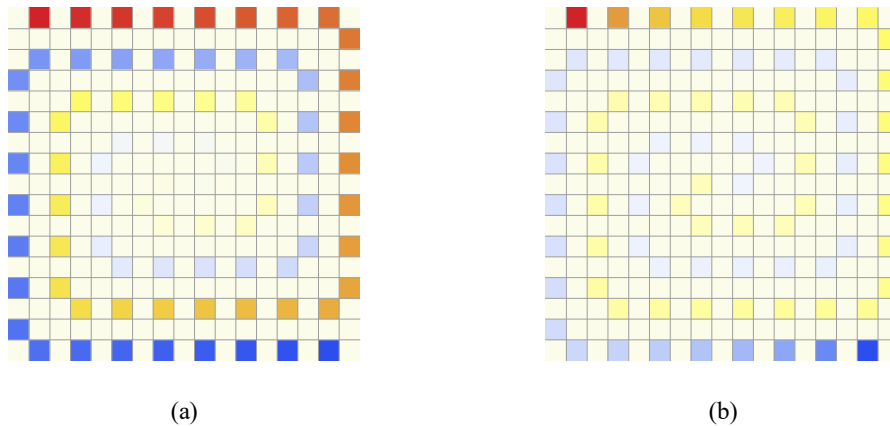


Figure 3: Order parameter $\langle S^z \rangle$ for (a) $q > 1$, and (b) $q = 1$. Warm color and cold colors denote respective spin up and down, and darker colors correspond to larger magnitude. The neutral muted shade represents 2D lattice sites not occupied by degrees of freedom of the 1D chain.

vertical in the east and west quadrant, and horizontal in the north and south quadrant. So the system indeed interact in both directions, leading to the 2D entanglement we have seen in the previous section regardless of the direction of bipartition. Furthermore, we show in this section that the layout of the 1D chain on the 2D lattice induces an antiferromagnetic order of the spin degree of freedom within each quadrant along the direction that there is no interaction.

The expectation value of the spin in a 1D chain has been computed for $q = 1$ from combinatorial methods [31, 32], field theoretic approach in the scaling limit [30], and the transfer matrix method [28]. All three approaches lead to the same scaling behavior as $r^{-1/2}$, where r is the distance from the closer boundary, with up spin on the first half, and down spin on the second. When twisted and embedded on the 2D lattice, an induced antiferromagnetic order appears with modulated amplitude that decays from the boundary to the center, as shown in 3 (b).

As was shown in Ref. [28], due to the opposite boundary conditions, the $q > 1$ ordered phase forms a domain wall between the two regions with positive and negative values of the order parameter. The correlation length in this case is reflected in the domain wall thickness ξ by

$$\langle S_k^z \rangle \propto \tanh \frac{N - k}{\xi}, \quad (10)$$

which can be derived from the Ginzburg-Landau theory [28]. The length scale depends on the deformation parameter as $\xi \propto 1/\log q$, which was obtained from numerical results by a matrix product state calculation [28]. Fig. 3 (a) depicts the twisting induced antiferromagnetic order in the direction orthogonal to 1D chain within each quadrant of the 2D lattice for $\xi = 2N$.

5 TN representation of the GS

The GS of the 1D Motzkin chain has a holographic TN representation [36], where each physical spin maps to a column of tensors sequentially contracted with neighbors above and below. The depth of the columns grows linearly from the boundaries of the chain to the center. Twisting the TN from the center results in a 2D TN for the GS of the present

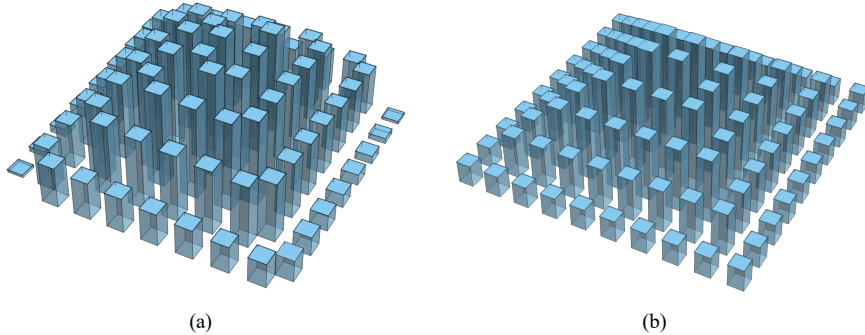


Figure 4: (a) TN representation of the 2D GS of the twisted Motzkin chain, where the contractions in the vertical direction are represented by placing the tensor cubes adjacent to each other, and in the horizontal planes, contraction only happens between neighbors along the twisted chain direction. (b) TN representation of the 2D GS of the coupled chain model, where contractions in each horizontal plane happen between neighboring tensor cubes in both directions.

model, which has a pyramid shape as shown in Fig. 4 (a). The geometry of the TN is globally the same as the 3D TN for the GS of the coupled Fredkin chain model [30] shown in Fig. 4 (b). But now the tensors in the bulk have only four internal legs instead of six. The number of bonds crossing the bipartition cut gives the correct scaling of the EE for the $q > 1$ phase of the colored model. At the critical point of the colorless model, the TN can be renormalized such that the depth of the columns grow logarithmically instead, giving the correct EE scaling in that case [27, 28].

The TN representation of the Motzkin and Fredkin GS defined in [36] actually gives an inverted step pyramid shaped network with the physical external legs at the bottom of each column of tensors. In this section, we define a new TN representation of the Fredkin GS with an upright pyramid shaped geometry, which consist of slightly sparser tensors. This TN is obtained using the tiling approach used in Ref. [36]. In this method the correspondence between spin configurations and walks is used to construct the TN representation. This is achieved through an intermediate step where a valid tiling of a set of tiles is associated to each walk present in the GS. In this context, a valid tiling is a tiling where each edge of each tile matches its adjacent tiles. By carefully choosing an appropriate set of tiles, one can assure a one-to-one correspondence between valid tilings and spin configurations present in the GS superposition. For spin configurations present in the GS of the Fredkin model, which are described by Dyck walks, this one-to-one correspondence can be assured by the set of tiles $B_i(c)$ seen in panel (a) of Fig. (5). In panel (b) and (c) we see that the valid tilings contain arrowed paths indicating the color correlation between spins in the given Dyck walk. A colored spin up (resp. down) at i is represented by a colored arrowed path entering (resp. leaving) the tiling at the floor edge of the bottom tile in the tower of tiles at i . Clearly, each valid tiling corresponds to a unique way of pairing the degrees of freedom. This set of tiles enables exactly one valid tiling for any given Dyck walk and no valid tiling for non-Dyck walks. To see this, note that by following the highest arrowed path within each tiling, the corresponding Dyck walk is traced out, see Fig. (5) (b) and (c). It is clear that a valid tiling for a given Dyck walk where this is not the case, is not possible. It is also clear that no valid tiling can be constructed for a non-Dyck walk, as that would necessarily violate arrow continuity at the step where the walk becomes negative (or at the endpoints if the walk starts or terminates at a non-zero

height). This establishes the one-to-one correspondence between valid tilings and the spin configurations in the ground state.

The tensor building up the TN representation is then defined by the set of tiles in the following way: The number of indices of the tensor is determined by the shape of the tiles and each tile represents an index configuration of the tensor giving a nonzero value. Contractions between two tensors in the TN, then correspond to summing over tile configurations matching at that edge. The tiles, valid tilings and the resulting TN, can be seen in [Fig. \(5\)](#).

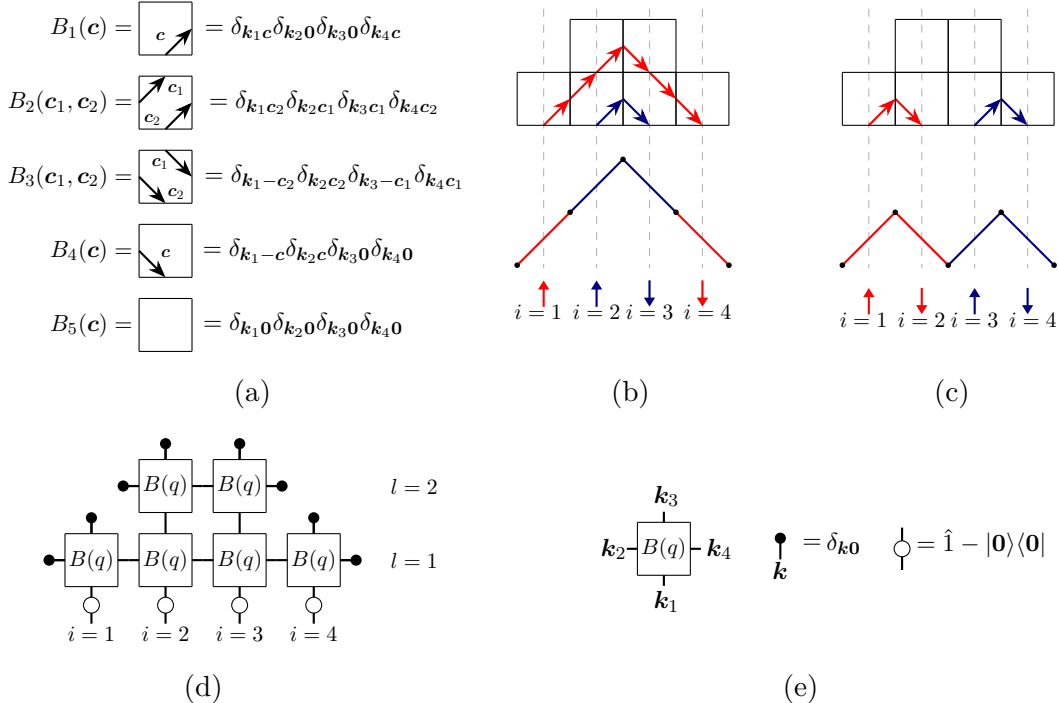


Figure 5: (a) The five different tiles $B_i(\mathbf{c})$ for the new Fredkin tensor network. The tiles are also defined as rank-4 tensors in terms of Kronecker deltas, where the indices \mathbf{k}_i are defined as for $B(q)$ in panel (d). We have $\mathbf{c} = (1, 0)$ for red arrow, $\mathbf{c} = (0, 1)$ for blue arrow. No arrow corresponds to $\mathbf{0}$. (b)-(c) Valid tilings corresponding to the maximal and minimal height Dyck walk for the $L = 4$ system. (d) TN representation of the ground state of the single Fredkin chain for $L = 4$. l denotes the different levels of the holographic TN. (e) The constituent tensors of the TN, where the white circle projects out the index value $\mathbf{0}$ corresponding to no arrow in the tilings.

The nonzero entries of the tensor in terms of the deformation parameter q are determined by counting the number of tiles in a tiling and considering the area under the corresponding Dyck walk. By weighing each tile with an appropriate value of the deformation parameter q , one can ensure that contracting the TN yields the weighted superposition of spin configurations in the GS. This gives a rank-4 tensor $B(q)$ as

$$B(q) = \sum_{\mathbf{c}_i=(1,0),(0,1)} [\sqrt{q}B_1(\mathbf{c}_1) + qB_2(\mathbf{c}_1, \mathbf{c}_2) + qB_3(\mathbf{c}_1, \mathbf{c}_2, \mathbf{c}_3, \mathbf{c}_4) + \sqrt{q}B_4(\mathbf{c}_1) + B_5(\mathbf{c}_1)]. \quad (11)$$

The indices $\mathbf{k}_1, \dots, \mathbf{k}_4$ of $B(q)$ are defined in panel (d) of [Fig. \(5\)](#) and have been suppressed in [Eq. \(11\)](#). We use a vector notation for the indices to keep track of the color of

the arrows, which is a notation conveniently extended to the tensors in the TN for the 2D systems [30]. It is clear that one can simply replace the different vectors with a unique number, to arrive at the more familiar way of denoting index configurations by numbers. Note also that we use a minus sign to indicate arrows leaving (resp. coming in) at the \mathbf{k}_1 (resp. \mathbf{k}_3) index. In Eq. (11), we consider two colors, namely red, $\mathbf{c} = (1, 0)$, and blue, $\mathbf{c} = (0, 1)$. Note that each of the tiles $B_i(\mathbf{c})$ can be defined as a rank-4 tensor expressed as a product of Kronecker deltas, as seen in panel (a) in Fig. (5). The shape of the resulting TN naturally becomes that of the valid tilings, giving an upright step pyramid shape as seen in panel (d) in Fig. (5). Note that the boundary tensors $\delta_{\mathbf{k},0}$ ensures that “no arrows flow out” of the TN, except at the bottom edges. Due to the tile without arrows, we must project out the index value corresponding to an empty edge at the bottom tile. We must therefore include projectors in the TN, as seen in Fig. (5) (d). This is similar to the rainbow TN presented with projectors in Ref. [36].

Finally, we mention that one can restrict the tensors at even and odd sites by taking into account that a Dyck walk can only reach an even (resp. odd) height after an even (resp. odd) number of steps. This implies that in valid tilings the tile above an even (resp. odd) position i , at an odd (resp. even) level l can never be the $B_1(\mathbf{c})$ tile, as that would correspond to a walk reaching an even height (resp. odd) after an odd (resp. even) number of steps. Due to the same reason the $B_4(\mathbf{c})$ tile can never be placed above an even (resp. odd) position, at an even (resp. odd) height. This means that one can build a TN where the tensors are built up of 4 tiles, instead of 5, at the expense of having two different tensors. One is $B(q)$ without $B_1(\mathbf{c})$ and the other one is $B(q)$ without $B_4(\mathbf{c})$. This gives a TN with slightly sparser tensor than the one presented in Ref. [36], at the cost of having two different tensors in the TN.

6 Conclusion

In this article, a frustration free 2D lattice Hamiltonian with exactly solvable GS that has volume scaling of EE is constructed by turning on the spatially anisotropic interaction following a specific path along which the degrees of freedom form a highly entangled Motzkin chain. The interaction is significantly simpler than the previous models of such highly entangled 2D systems realized by coupling arrays of highly entangled chains. Similar constructions of 2D entanglement from twisting 1D chains can be applied to the highly entangled XX chain with inhomogeneous coupling [8–10]. The volume scaling of EE in 2D is possible since the entangling color degree of freedom tend to form Bell pairs with their point reflection partner about the center of the system. Hence, at the moment, it is not clear if similar nontrivial construction works for 3D systems, for which an inversion symmetric path traversing all lattice points in the 3D space has to be specified. On the other hand, the coupled chains construction in principle works in any dimension via tiling. These alternative examples of area-law violating GSs provide a better understanding of the interplay between EE and spectral gap scaling, or the tradeoff between quantum computing resource and robustness against noise. The ultimate goal in this direction is to generalize the area law to gapless ground states to get a relation between the rate of decay in spectral gap and growth of EE with the system size.

Acknowledgements

ZZ thanks Shankar Balasubramanian, Soonwan Choi, Israel Klich, and Ethan Lake for discussions.

A Typical height change in a segment of Motzkin path

In this appendix, we determine the typical height change in a segment of Motzkin path by finding the most probable height change using combinatorics. The number of Motzkin path segments that start at height h_i and end at height h_f over a horizontal distance of x can be enumerated using André's reflection method, see Fig. (6). Such paths meeting the Motzkin condition of non-negative height everywhere is equal to the total number of random walks subtracted by those that does reach height -1 somewhere. The latter are in one-to-one mapping with paths that are mirror images about the horizontal line $h = -1$ after the first time the path reaches height -1 . These paths are in turn enumerated by the random walks from height h_i to height $-h_f - 2$.

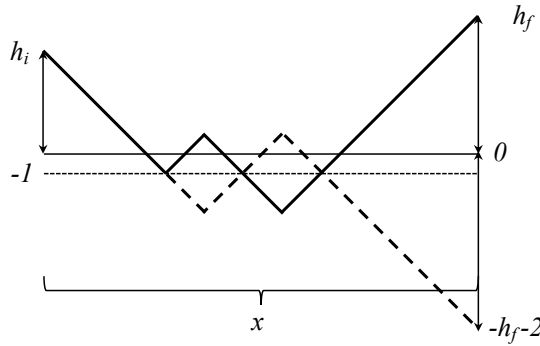


Figure 6: The number of segments of Motzkin paths that start at height h_i and end at height h_f over x steps without having negative heights in the middle can be enumerated with André's reflection method.

For simplicity, we first count such Dyck paths, which are Motzkin paths without the option of flat moves, as

$$\sqrt{p_D(h_f, h_i, x)} = \binom{x}{\frac{x+h_f-h_i}{2}} - \binom{x}{\frac{x+h_f+h_i}{2} + 1} \approx \sqrt{\frac{2}{\pi x}} 2^x \left(e^{-\frac{(h_f-h_i)^2}{x}} - e^{-\frac{(h_f+h_i)^2}{x}} \right) \quad (\text{A.1})$$

where the limit $x \gg h_i, h_f \gg 1$ has been used. The most probable height change $h_f^* - h_i$ is determined by $p'_D(h_f^*, h_i, x) = 0$, which is solved from

$$e^{\frac{4h_i h_f^*}{x}} = \frac{h_f^* + h_i}{h_f^* - h_i}. \quad (\text{A.2})$$

Motzkin paths starting and ending at finite height can be counted analogously, resulting in

$$\sqrt{p_M(h_f, h_i, x)} \propto e^{-\frac{3(h_f-h_i)^2}{2x}} - e^{-\frac{3(h_f+h_i)^2}{2x}}, \quad (\text{A.3})$$

and the typical height change determined by

$$e^{\frac{6h_i h_f^*}{x}} = \frac{h_f^* + h_i}{h_f^* - h_i}. \quad (\text{A.4})$$

The leading contribution to EE is proportional to the total net height change between the two subsystems

$$S \sim \sum_{i=0}^{\frac{L}{2}-1} |\langle h_{2i+1} - h_{2i} \rangle| \propto \int \mathcal{D}[h] \left[\sum_{k=1}^{\frac{L}{2}} (-1)^k h_{k-1} + \sum_{k=\frac{L}{2}}^{L-1} (-1)^k h_k \right], \quad (\text{A.5})$$

where h_i are the height variable at the L endpoints of the segments resulting from the bipartition on the 2D lattice. In the second form of the equation the contribution from the segments lying in the first half of the chain and contributions from segments lying in the second half of the chain have been split into two sums, using that in the first half of the chain the height increases, while in the second half of the chain it decreases. Throughout the paper, L assumed an integer multiple of 4 without loss of generality. The functional integral over the height configuration $h(x)$ is done by integrating over the height variable at discrete locations weighted by corresponding probabilities

$$\mathcal{D}[h] = p(h_1) \prod_{i=1}^{\frac{L}{2}-1} dh_i p(h_{i+1}, h_i, |4i-2L|) \prod_{j=\frac{L}{2}}^{L-2} dh_j p(h_{j+1}, h_j, |4(j+1)-2L|) p(h_{L-1}), \quad (\text{A.6})$$

with the probability distribution of boundary segments are given by [11, 14]

$$p(h) = \begin{cases} \frac{2^{4L+3}h^2}{\pi x} e^{-\frac{h^2}{L}}, & \text{for Dyck paths,} \\ \frac{2^{4L+3}h^2}{\pi x} e^{-\frac{3h^2}{2L}}, & \text{for Motzkin paths.} \end{cases} \quad (\text{A.7})$$

References

- [1] D. N. Page, *Average entropy of a subsystem*, Phys. Rev. Lett. **71**, 1291 (1993), doi:[10.1103/PhysRevLett.71.1291](https://doi.org/10.1103/PhysRevLett.71.1291).
- [2] J. Eisert, M. Cramer and M. B. Plenio, *Colloquium: Area laws for the entanglement entropy*, Reviews of Modern Physics **82**(1), 277–306 (2010), doi:[10.1103/revmodphys.82.277](https://doi.org/10.1103/revmodphys.82.277).
- [3] M. B. Hastings and T. Koma, *Spectral gap and exponential decay of correlations*, Communications in Mathematical Physics **265**(3), 781–804 (2006), doi:[10.1007/s00220-006-0030-4](https://doi.org/10.1007/s00220-006-0030-4).
- [4] A. Anshu, I. Arad and D. Gosset, *An area law for 2d frustration-free spin systems*, In *Proceedings of the 54th Annual ACM SIGACT Symposium on Theory of Computing*, STOC '22. ACM, doi:[10.1145/3519935.3519962](https://doi.org/10.1145/3519935.3519962) (2022).
- [5] C. Holzhey, F. Larsen and F. Wilczek, *Geometric and renormalized entropy in conformal field theory*, Nuclear Physics B **424**(3), 443 (1994), doi:[https://doi.org/10.1016/0550-3213\(94\)90402-2](https://doi.org/10.1016/0550-3213(94)90402-2).
- [6] P. Calabrese and J. Cardy, *Entanglement entropy and conformal field theory*, Journal of Physics A: Mathematical and Theoretical **42**(50), 504005 (2009), doi:[10.1088/1751-8113/42/50/504005](https://doi.org/10.1088/1751-8113/42/50/504005).
- [7] D. Gioev and I. Klich, *Entanglement entropy of fermions in any dimension and the widom conjecture*, Phys. Rev. Lett. **96**, 100503 (2006), doi:[10.1103/PhysRevLett.96.100503](https://doi.org/10.1103/PhysRevLett.96.100503).

- [8] G. Vitagliano, A. Riera and J. I. Latorre, *Volume-law scaling for the entanglement entropy in spin-1/2 chains*, New Journal of Physics **12**(11), 113049 (2010), doi:[10.1088/1367-2630/12/11/113049](https://doi.org/10.1088/1367-2630/12/11/113049).
- [9] G. Ramírez, J. Rodríguez-Laguna and G. Sierra, *From conformal to volume law for the entanglement entropy in exponentially deformed critical spin 1/2 chains*, Journal of Statistical Mechanics: Theory and Experiment **2014**(10), P10004 (2014), doi:[10.1088/1742-5468/2014/10/P10004](https://doi.org/10.1088/1742-5468/2014/10/P10004).
- [10] G. Ramírez, J. Rodríguez-Laguna and G. Sierra, *Entanglement over the rainbow*, Journal of Statistical Mechanics: Theory and Experiment **2015**(6), P06002 (2015), doi:[10.1088/1742-5468/2015/06/P06002](https://doi.org/10.1088/1742-5468/2015/06/P06002).
- [11] S. Bravyi, L. Caha, R. Movassagh, D. Nagaj and P. W. Shor, *Criticality without frustration for quantum spin-1 chains*, Phys. Rev. Lett. **109**, 207202 (2012), doi:[10.1103/PhysRevLett.109.207202](https://doi.org/10.1103/PhysRevLett.109.207202).
- [12] R. Movassagh and P. W. Shor, *Supercritical entanglement in local systems: Counterexample to the area law for quantum matter*, Proceedings of the National Academy of Sciences **113**(47), 13278 (2016), doi:[10.1073/pnas.1605716113](https://doi.org/10.1073/pnas.1605716113).
- [13] L. Dell'Anna, O. Salberger, L. Barbiero, A. Trombettoni and V. E. Korepin, *Violation of cluster decomposition and absence of light cones in local integer and half-integer spin chains*, Phys. Rev. B **94**, 155140 (2016), doi:[10.1103/PhysRevB.94.155140](https://doi.org/10.1103/PhysRevB.94.155140).
- [14] O. Salberger and V. Korepin, *Fredkin Spin Chain*, pp. 439–458, WORLD SCIENTIFIC, doi:[10.1142/9789813233867_0022](https://doi.org/10.1142/9789813233867_0022) (2018).
- [15] Z. Zhang, A. Ahmadain and I. Klich, *Novel quantum phase transition from bounded to extensive entanglement*, Proceedings of the National Academy of Sciences **114**(20), 5142 (2017), doi:[10.1073/pnas.1702029114](https://doi.org/10.1073/pnas.1702029114).
- [16] O. Salberger, T. Udagawa, Z. Zhang, H. Katsura, I. Klich and V. Korepin, *Deformed Fredkin spin chain with extensive entanglement*, Journal of Statistical Mechanics: Theory and Experiment **6**(6), 063103 (2017), doi:[10.1088/1742-5468/aa6b1f, 1611.04983](https://doi.org/10.1088/1742-5468/aa6b1f).
- [17] Z. Zhang and I. Klich, *Entropy, gap and a multi-parameter deformation of the fredkin spin chain*, Journal of Physics A: Mathematical and Theoretical **50**(42), 425201 (2017), doi:[10.1088/1751-8121/aa866e](https://doi.org/10.1088/1751-8121/aa866e).
- [18] Z. Zhang, *Entanglement blossom in a simplex matryoshka*, Annals of Physics **457**, 169395 (2023), doi:<https://doi.org/10.1016/j.aop.2023.169395>.
- [19] S. Balasubramanian, E. Lake and S. Choi, *2d hamiltonians with exotic bipartite and topological entanglement* (2023), [2305.07028](https://arxiv.org/abs/2305.07028).
- [20] Z. Zhang, *Bicolor loop models and their long range entanglement*, Quantum **8**, 1268 (2024), doi:[10.22331/q-2024-02-29-1268](https://doi.org/10.22331/q-2024-02-29-1268).
- [21] Z. Zhang and I. Klich, *Coupled Fredkin and Motzkin chains from quantum six- and nineteen-vertex models*, SciPost Phys. **15**, 044 (2023), doi:[10.21468/SciPostPhys.15.2.044](https://doi.org/10.21468/SciPostPhys.15.2.044).
- [22] Z. Zhang and I. Klich, *Quantum lozenge tiling and entanglement phase transition*, Quantum **8**, 1497 (2024), doi:[10.22331/q-2024-10-10-1497](https://doi.org/10.22331/q-2024-10-10-1497).

[23] S. Sahoo, Z. Zhang and J. C. Y. Teo, *Coupled wire model of symmetric majorana surfaces of topological superconductors*, Phys. Rev. B **94**, 165142 (2016), doi:[10.1103/PhysRevB.94.165142](https://doi.org/10.1103/PhysRevB.94.165142).

[24] W. Zhang, *Sequential generation of two-dimensional super-area-law states with local parent hamiltonian* (2025), [2505.02914](https://arxiv.org/abs/2505.02914).

[25] A. G. Pronko, *Periodic motzkin chain: Ground states and symmetries*, Nuclear Physics B **1017**, 116963 (2025), doi:<https://doi.org/10.1016/j.nuclphysb.2025.116963>.

[26] A. G. Pronko, *Periodic motzkin chain: Ground states and symmetries*, Nuclear Physics B **1017**, 116963 (2025), doi:<https://doi.org/10.1016/j.nuclphysb.2025.116963>.

[27] R. N. Alexander, G. Evenbly and I. Klich, *Exact holographic tensor networks for the Motzkin spin chain*, Quantum **5**, 546 (2021), doi:[10.22331/q-2021-09-21-546](https://arxiv.org/abs/2021.09.21-546).

[28] O. B. Mykland and Z. Zhang, *Reconciling translational invariance and hierarchy* (2025), [2507.14656](https://arxiv.org/abs/2507.14656).

[29] K. Okuyama, *Holographic tensor network for double-scaled SYK*, SciPost Phys. **19**, 083 (2025), doi:[10.21468/SciPostPhys.19.4.083](https://doi.org/10.21468/SciPostPhys.19.4.083).

[30] O. B. Mykland and Z. Zhang, *Highly entangled 2d ground states: Tensor networks and correlation functions* (2025), [2502.20192](https://arxiv.org/abs/2502.20192).

[31] R. Movassagh, *Entanglement and correlation functions of the quantum motzkin spin-chain*, Journal of Mathematical Physics **58**(3), 031901 (2017), doi:[10.1063/1.4977829](https://doi.org/10.1063/1.4977829), https://pubs.aip.org/aip/jmp/article-pdf/doi/10.1063/1.4977829/15803346/031901_1_online.pdf.

[32] V. Menon, A. Gu and R. Movassagh, *Symmetries, correlation functions, and entanglement of general quantum motzkin spin-chains* (2024), [2408.16070](https://arxiv.org/abs/2408.16070).

[33] Z. Zhang and H. Schou Røising, *The frustration-free fully packed loop model*, Journal of Physics A: Mathematical and Theoretical **56**(19), 194001 (2023), doi:[10.1088/1751-8121/acc76f](https://doi.org/10.1088/1751-8121/acc76f).

[34] L. Levine and R. Movassagh, *The gap of the area-weighted motzkin spin chain is exponentially small*, Journal of Physics A: Mathematical and Theoretical **50**(25), 255302 (2017), doi:[10.1088/1751-8121/aa6cc4](https://doi.org/10.1088/1751-8121/aa6cc4).

[35] R. Andrei, M. Lemm and R. Movassagh, *The spin-one motzkin chain is gapped for any area weight $t < 1$* (2022), [2204.04517](https://arxiv.org/abs/2204.04517).

[36] R. N. Alexander, A. Ahmadain, Z. Zhang and I. Klich, *Exact rainbow tensor networks for the colorful motzkin and fredkin spin chains*, Phys. Rev. B **100**, 214430 (2019), doi:[10.1103/PhysRevB.100.214430](https://doi.org/10.1103/PhysRevB.100.214430).